This copy of the ESI replaces the previous version published on 15 Dec 2022

Supplementary Information

Magnetic field effects on radical pair reactions: estimation of $B_{1/2}$ for flavin-tryptophan radical pairs in cryptochromes

Siu Ying Wong[1#], Philip Benjamin[2#] and P. J. Hore[2]*

[1] Institut für Physik, Carl-von-Ossietzky Universität Oldenburg, Oldenburg 26111, Germany

[2] Department of Chemistry, University of Oxford, Oxford, OX1 3QZ, UK

[#] These authors contributed equally

*Author for correspondence

Contents

S1. Re-analysis of $B_{1/2}$ data in Weller *et al.*

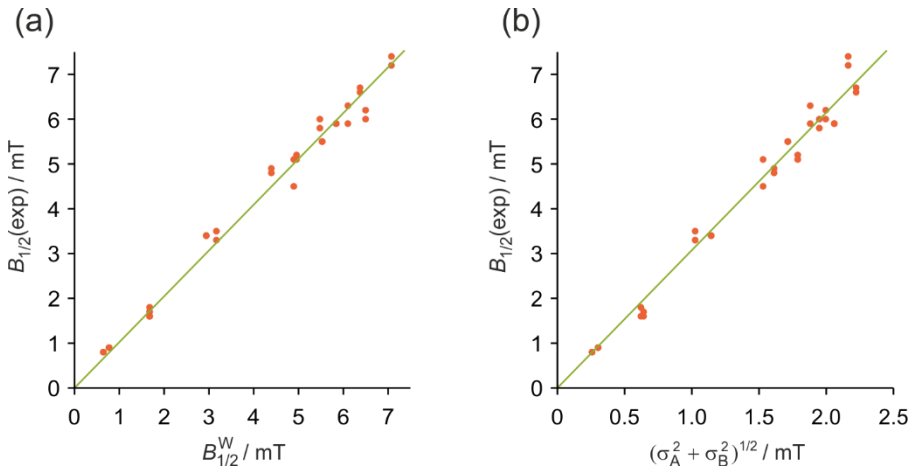

Fig. S1. Analysis of experimental $B_{1/2}$ data (Table 1 of Ref. [1]) for photo-induced electron transfer reactions of pyrene-h_{10} or pyrene-d_{10} with a variety of aromatic electron donors. (a) Experimental $B_{1/2}$ values plotted against $B^{W}_{1/2}$. The green line is the best linear fit: $B_{1/2}(\text{exp}) = 1.03B^{W}_{1/2}$. Correlation coefficient: R = 0.993. (b) The same data plotted against $\left(\sigma_A^2 + \sigma_B^2\right)^{1/2}$ with best linear fit: $B_{1/2}(\text{exp}) = 3.07\left(\sigma_A^2 + \sigma_B^2\right)^{1/2}$. Correlation coefficient: R = 0.990.

S2. Hyperfine interactions

Nucleus	Hyperfine tensor / mT			Isotropic coupling / mT
WHB1	1.572	0.016	0.047	1.605
	0.016	1.516	0.063	
	0.047	0.063	1.726	
FN5	–0.099	–0.003	0.000	0.523
	–0.003	–0.087	0.000	
	0.000	0.000	1.757	
WHE1	–1.001	0.206	0.193	–0.598
	0.206	–0.442	0.307	
	0.193	0.307	–0.352	
WNE1	–0.053	0.059	–0.046	0.322
	0.059	0.564	–0.565	
	–0.046	–0.565	0.453	
WHE3	–0.571	0.161	0.196	–0.488
	0.161	–0.484	0.084	
	0.196	0.084	–0.408	
FH81, FH82, FH83	0.440	0.000	0.000	0.440
	0.000	0.440	0.000	
	0.000	0.000	0.440	
FN10	–0.015	–0.002	0.000	0.189
	–0.002	–0.024	0.000	
	0.000	0.000	0.605	
FH1', FH1''	0.407	0.000	0.000	0.407
	0.000	0.407	0.000	
	0.000	0.000	0.407	
FH6	–0.201	0.033	0.000	–0.387
	0.033	–0.527	0.000	
	0.000	0.000	–0.434	
WHZ2	–0.443	0.127	0.149	–0.364
	0.127	–0.354	0.095	
	0.149	0.095	–0.294	
WHD1	–0.275	–0.157	–0.175	–0.278
	–0.157	–0.273	0.092	
	–0.175	0.092	–0.285	
WN	0.137	0.024	–0.006	0.146
	0.024	0.176	–0.012	
	–0.006	–0.012	0.127	
WHH2	–0.043	–0.074	–0.068	–0.208
	–0.074	–0.279	–0.032	
	–0.068	–0.032	–0.303	

FH71, FH72, FH73	–0.142	0.000	0.000	–0.142
	0.000	–0.142	0.000	
	0.000	0.000	–0.142	
WHA	–0.054	–0.001	–0.007	–0.093
	–0.001	–0.037	0.047	
	–0.007	0.047	–0.189	
FN3	–0.043	0.000	0.000	–0.038
	0.000	–0.033	0.000	
	0.000	0.000	–0.039	
FH9	0.067	–0.025	0.000	0.057
	–0.025	0.108	0.000	
	0.000	0.000	–0.005	
WHB2	0.158	–0.008	0.039	0.046
	–0.008	–0.017	0.014	
	0.039	0.014	–0.004	
WHZ3	0.010	–0.064	–0.066	–0.040
	–0.064	–0.065	0.037	
	–0.066	0.037	–0.065	
FH3	–0.030	–0.003	0.000	–0.019
	–0.003	0.038	0.000	
	0.000	0.000	–0.065	
WHN	0.0182	0.0548	–0.0222	–0.007
	0.0548	0.0272	–0.0238	
	–0.0222	–0.0238	–0.0261	
FN1	–0.026	0.003	0.000	–0.003
	0.003	–0.023	0.000	
	0.000	0.000	0.038	

Table S1. Hyperfine coupling parameters of magnetic nuclei in $FAD^{\bullet-}$ (F) and $TrpH^{\bullet+}$ (W), in order of inclusion in the quantum dynamics (QD) and improved semiclassical (SC) simulations. Standard PDB/IUPAC nomenclature is used, with the labelling scheme given in Fig. S2. Calculations were performed (by Dr Ilya Kuprov, Department of Chemistry, University of Southampton) using density functional theory in Gaussian-03[2] at the UB3LYP/EPR-III level, for the radical anion of 7,8,10-trimethyl isoalloxazine (lumiflavin) in the case of $FAD^{\bullet-}$ and the radical cation of a free tryptophan amino acid in the case of $TrpH^{\bullet+}$.[3]

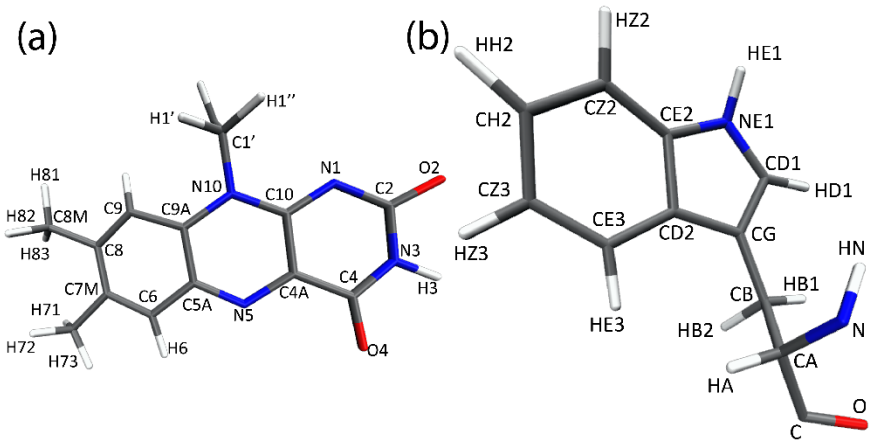

Fig. S2. Atom labelling schemes for (a) FAD and (b) TrpH radicals.

S3. Computational methods

Schulten-Wolynes semiclassical method (SW)

Magnetic field effects were calculated as originally described by Schulten and Wolynes[4] with Monte-Carlo averaging over isotropic hyperfine fields in the two radicals.[5] The spin Hamiltonian was of the form $\hat{H} = \hat{H}_\mathrm{A} + \hat{H}_\mathrm{B}$, with:

$$\hat{H}_\mathrm{Q} = \omega \hat{S}_{\mathrm{Q}z} + \sum_{j=x,y,z} h_{\mathrm{Q}j} \hat{S}_{\mathrm{Q}j},$$

in which the first term accounts for the electron Zeeman interaction ($\omega = -\gamma_\mathrm{e} B$) and the second the hyperfine interactions. $\hat{S}_{\mathrm{Q}j}$ is the *j*-component of the electron spin operator for radical Q. The hyperfine fields, $h_{\mathrm{Q}j}$, were chosen randomly from normal distributions with mean zero and standard deviation σ_Q. The triplet yield was obtained as:[6]

$$\Phi_\mathrm{T}(B) = 1 - \sum_{n=1}^{4}\sum_{m=1}^{4} \left|\langle n|\hat{P}^\mathrm{S}|m\rangle\right|^2 \frac{k^2}{k^2 + (\omega_n - \omega_m)^2},$$

where ω_n and ω_m are eigenvalues of $\hat{H}$, $|n\rangle$ and $|m\rangle$ are the corresponding eigenstates, and $\hat{P}^\mathrm{S}$ is the singlet projection operator:

$$\hat{P}^\mathrm{S} = \frac{1}{4}\hat{E} - \sum_{j=x,y,z} \hat{S}_{\mathrm{A}j}\hat{S}_{\mathrm{B}j}.$$

50,000 Monte-Carlo averages were used for each calculation of the triplet yield in Fig. 2. $B_{1/2}$ was obtained by interpolating $\Phi_\mathrm{T}(B)$ (Section S4).

Exact quantum spin dynamics method (QD)

The spin Hamiltonian was again of the form $\hat{H} = \hat{H}_\mathrm{A} + \hat{H}_\mathrm{B}$, but now with

$$\hat{H}_\mathrm{Q} = \omega \hat{S}_{\mathrm{Q}z} + \sum_i a_{\mathrm{Q}i}\, \hat{\mathbf{S}}_\mathrm{Q} \cdot \hat{\mathbf{I}}_{\mathrm{Q}i}$$

in which $a_{\mathrm{Q}i}$ and $\hat{\mathbf{I}}_{\mathrm{Q}i}$ are respectively the isotropic hyperfine coupling constant and the nuclear spin operator of nucleus *i* in radical Q. The triplet yield was calculated as:[7]

$$\Phi_\mathrm{T} = \frac{3}{4} - \frac{1}{Z}\sum_p\sum_q\sum_n\sum_m\sum_r\sum_s \left(\hat{S}_{\mathrm{A}q}\right)_{nm}\left(\hat{S}_{\mathrm{A}p}\right)_{mn}\left(\hat{S}_{\mathrm{B}q}\right)_{rs}\left(\hat{S}_{\mathrm{B}p}\right)_{sr} \frac{k^2}{k^2 + (\omega_m^{(\mathrm{A})} - \omega_n^{(\mathrm{A})} + \omega_s^{(\mathrm{B})} - \omega_r^{(\mathrm{B})})^2}$$

where $p, q \in \{x, y, z\}$, *n*, *m* and *r*, *s* label the eigenstates of $\hat{H}_\mathrm{A}$ and $\hat{H}_\mathrm{B}$, respectively, with eigenvalues $\omega_n^{(\mathrm{A})}$, $\omega_m^{(\mathrm{A})}$, $\omega_r^{(\mathrm{B})}$, and $\omega_s^{(\mathrm{B})}$, and $\left(\hat{S}_{\mathrm{A}q}\right)_{nm} = \langle n|\hat{S}_{\mathrm{A}q}|m\rangle$, etc. Z is the product of the dimensions of the nuclear Hilbert spaces of the two radicals. $B_{1/2}$ was obtained by interpolating $\Phi_\mathrm{T}(B)$ (Section S4). The calculations were performed using MolSpin.[8]

Quantum mechanical Monte-Carlo method (QMMC)

Calculations were performed using the QD method outlined above. The hyperfine coupling constants were chosen as described in the main text. 1500 radical pairs were simulated for each of the histograms in Fig. 3. $B_{1/2}$ was obtained by interpolating $\Phi_{\mathrm{T}}(B)$ (Section S4).

Improved semiclassical method (SC)

Magnetic field effects were calculated as originally described by Manolopoulos and Hore[9] and concisely summarised by Fay et al.[10] The magnetic fields used for the interpolation procedure (Section S4) are given in Table S2. In each case, the singlet probability was integrated over $0 \le t \le T$ with $T = 10/k$ and time-step $\Delta t = T/10^4$. All calculations used a minimum of 10^6 Monte-Carlo samples.

k / s^{-1}	B / mT
1×10^6 (isotropic)	0, 1.4, 1.8, 2.2, 2.6, 1000
1×10^6 (anisotropic)	0, 2.0, 2.4, 2.8, 3.2, 1000
1×10^7	0, 1.4, 1.8, 2.2, 2.6, 1000
1×10^8	0, 1.9, 2.3, 2.7, 3.1, 1000
3×10^8	0, 2.7, 3.1, 3.5, 3.9, 1000
5×10^8	0, 3.6, 4.0, 4.4, 4.8, 1000
1×10^9	0, 5.8, 6.2, 6.6, 7.0, 1000

Table S2. Magnetic field strengths chosen for the interpolation procedure for the recombination rate constants in Fig. 4.

Stochastic Schrödinger equation method (*SU*(*Z*))

The spin Hamiltonian in this case was of the general form $\hat{H} = \hat{H}_{\mathrm{A}} + \hat{H}_{\mathrm{B}} + \hat{H}_{\mathrm{AB}}$, with

$$\hat{H}_{\mathrm{Q}} = \omega \hat{S}_{\mathrm{Qz}} + \sum_i \hat{\mathbf{S}}_{\mathrm{Q}} \cdot \mathbf{A}_{\mathrm{Q}i} \cdot \hat{\mathbf{I}}_{\mathrm{Q}i},$$

$$\hat{H}_{\mathrm{AB}} = \hat{\mathbf{S}}_{\mathrm{A}} \cdot \mathbf{D} \cdot \hat{\mathbf{S}}_{\mathrm{B}}.$$

$\mathbf{A}_{\mathrm{Q}i}$ is the hyperfine interaction tensor of nucleus i in radical Q and $\mathbf{D}$ is the dipolar coupling tensor, appropriate for FAD and Trp318 in pigeon cryptochrome 4a:

$$\mathbf{D} / \mathrm{mT} = \begin{pmatrix} 0.039 & -0.432 & 0.175 \\ -0.432 & -0.279 & 0.251 \\ 0.175 & 0.251 & 0.239 \end{pmatrix}.$$

For the simulations with isotropic hyperfine interactions, $\mathbf{A}_{\mathrm{Q}i} = diag(a_{\mathrm{Q}i}, a_{\mathrm{Q}i}, a_{\mathrm{Q}i})$.

Magnetic field effects were calculated as described by Fay et al.[11] In each case, a single *SU*(*Z*) state was propagated using the Short Iterative Lanczos method,[12] with a Krylov subspace dimension of $p = 15$. The vector of Krylov subspace coefficients $\boldsymbol{c}(t)$ was propagated according to

$$\mathbf{c}(t + \mathrm{d}t) = \mathrm{e}^{-\mathrm{i}\mathbf{A}\mathrm{d}t}\mathbf{c}(t),$$

where **A** is the Krylov subspace representation of the spin Hamiltonian generated via the Lanczos method. A new Krylov subspace was generated whenever the condition $c_{p-1}(t)/|\mathbf{c}| \geq 10^{-5}$ was met. For all *SU*(*Z*) calculations, the maximum integration time was 5 μs, using a timestep of 1 ns.

S4. Interpolation of $\Phi_T(B)$ to obtain $B_{1/2}$

Method	*B* values for calculation of $\Phi_T(B)$	Fitting function used for interpolation
SW	21 values equally spaced between 0 and 10 mT	3rd order polynomial
QMMC	20 values logarithmically spaced between 0.1 and 10 mT	3rd degree spline
QD	$n_{nuc} \leq 12$: 500 values logarithmically spaced between 10^{-11} and 10 mT $n_{nuc} \geq 13$: 21 values spanning 1 mT, centred at the $B_{1/2}$ value for $n_{nuc} - 1$	
SC	1.4, 1.8, 2.2 and 2.6 mT	2nd order polynomial
SU(*Z*)	Isotropic: 1.4, 1.8, 2.2 and 2.6 mT Anisotropic: 2.0, 2.4, 2.8 and 3.2 mT	4th order polynomial

Table S3. Summary of parameters and fitting functions used in the interpolation procedures to obtain $B_{1/2}$ for the different simulation methods. In every case $\Phi_T(B_{1/2})$ was obtained as:

$$\Phi_T(B_{1/2}) = \frac{\Phi_T(B=0) + \Phi_T(B=1.0\,\mathrm{T})}{2}.$$

S5. Simulated magnetic field effects: SW method

Field-dependence of $\Phi_T(B)$

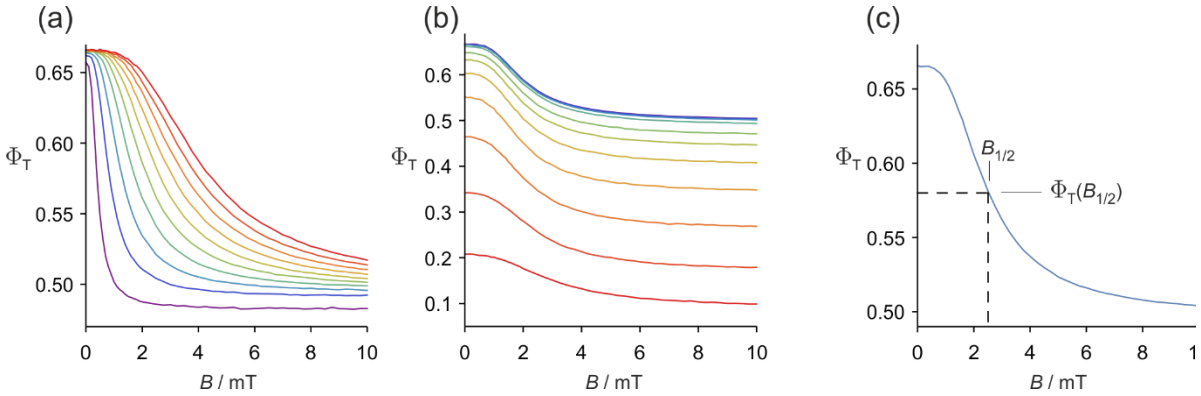

Fig. S3. (a) Magnetic field effects (SW method) from which the $B_{1/2}$ values in Fig. 2a were obtained by interpolation. σ_{AB} = 0.2 mT (violet) to 2.0 mT (red) in steps of 0.2 mT. (b) Simulated magnetic field effects from which the $B_{1/2}$ values in Fig. 2c were obtained by interpolation. k = $10^{5.0}$, $10^{5.5}$, $10^{6.0}$, $10^{6.5}$, $10^{7.0}$, $10^{7.25}$, $10^{7.5}$, $10^{7.75}$, $10^{8.0}$, $10^{8.25}$, $10^{8.5}$ s^{-1} (violet to red) (c) Simulated magnetic field effect from which $B_{1/2}$ = 2.51 mT (Table 1) was obtained by interpolation.

Dependence of $B_{1/2}$ on σ_{AB} and σ_A/σ_B for various recombination rates

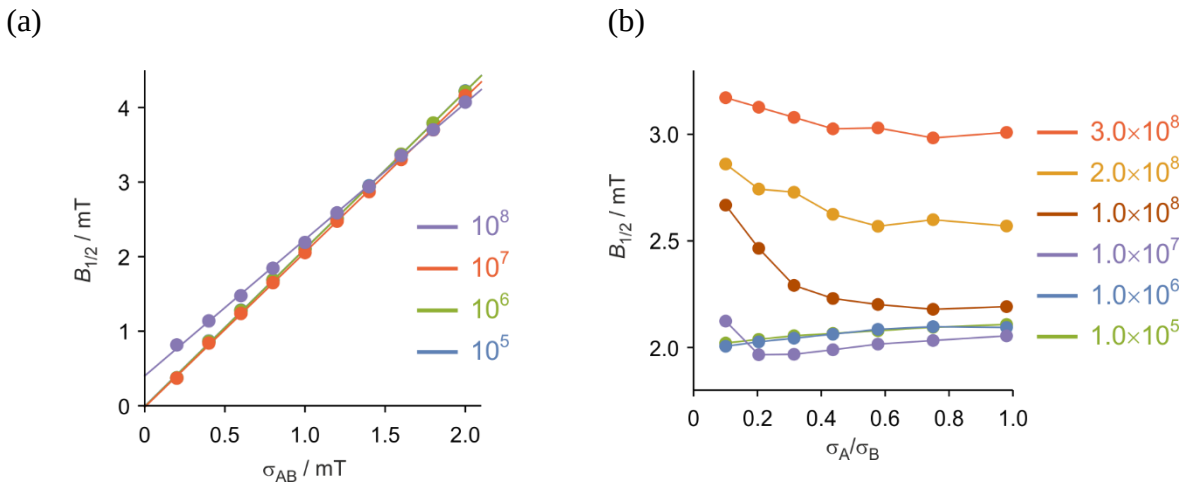

Fig. S4. (a) $B_{1/2}$ (SW method) plotted as a function of σ_{AB} for σ_A = σ_B for different values of the recombination rate constant, k (in s^{-1}), as indicated. Apart from $k = 10^8$ s^{-1}, $B_{1/2} \approx 2.11\,\sigma_{AB}$. (b) $B_{1/2}$ (SW method) plotted as a function of σ_A/σ_B for σ_{AB} = 1 mT and different values of the recombination rate constant, k (in s^{-1}), as indicated. $B_{1/2}$ increases markedly when $k \geq 10^7$ s^{-1}.

Dependence of $B_{1/2}$ on k

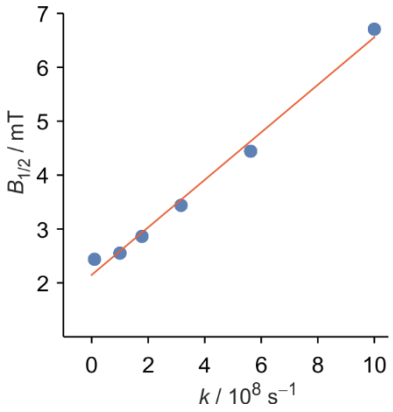

Fig. S5. $B_{1/2}$ (SW method) plotted as a function of k for σ_A = 0.70 mT and σ_B = 0.97 mT. The line is the best linear fit: $B_{1/2}$ / mT $\approx 2.15 + k / (2.27 \times 10^8\ \mathrm{s}^{-1})$. Although the dependence of $B_{1/2}$ on k here is not as linear as for the SC calculation (Fig. 4b), the gradient is similar.

S6. Simulated magnetic field effects: QMMC method

Field-dependence of $\Phi_T(B)$

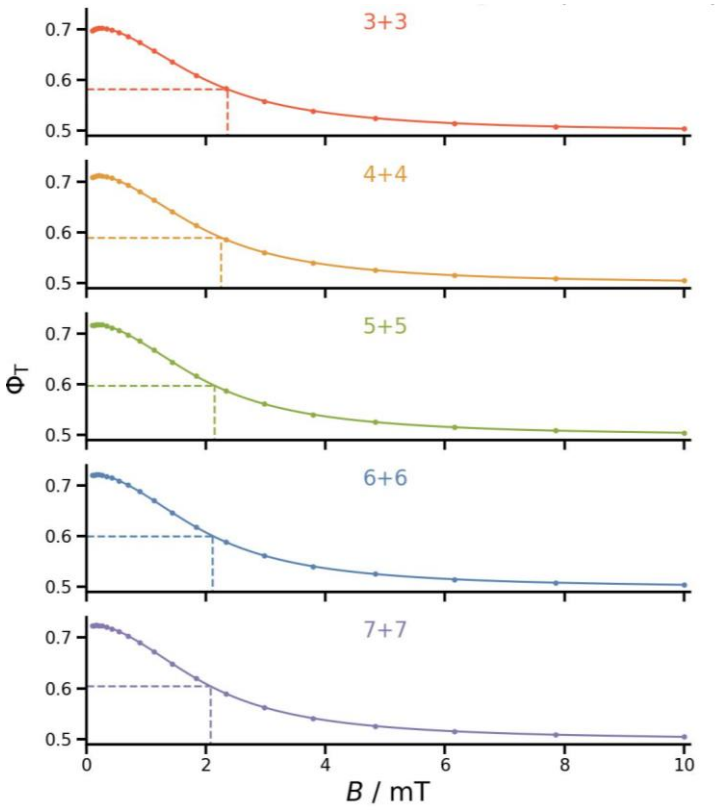

Fig. S6. Magnetic field effects (QMMC method). Each panel shows the average of 1500 calculations of $\Phi_T(B)$ for $k = 10^6$ s^{-1} for model [FAD$^{\bullet-}$ TrpH$^{\bullet+}$] radical pairs containing 3, 4, 5, 6, or 7 spin-½ hyperfine interactions per radical. Solid lines: 3rd degree spline fits to the calculated values of Φ_T (B) (dots). Dashed lines: interpolations used to obtain $B_{1/2}$ values.

Additional QMMC histograms

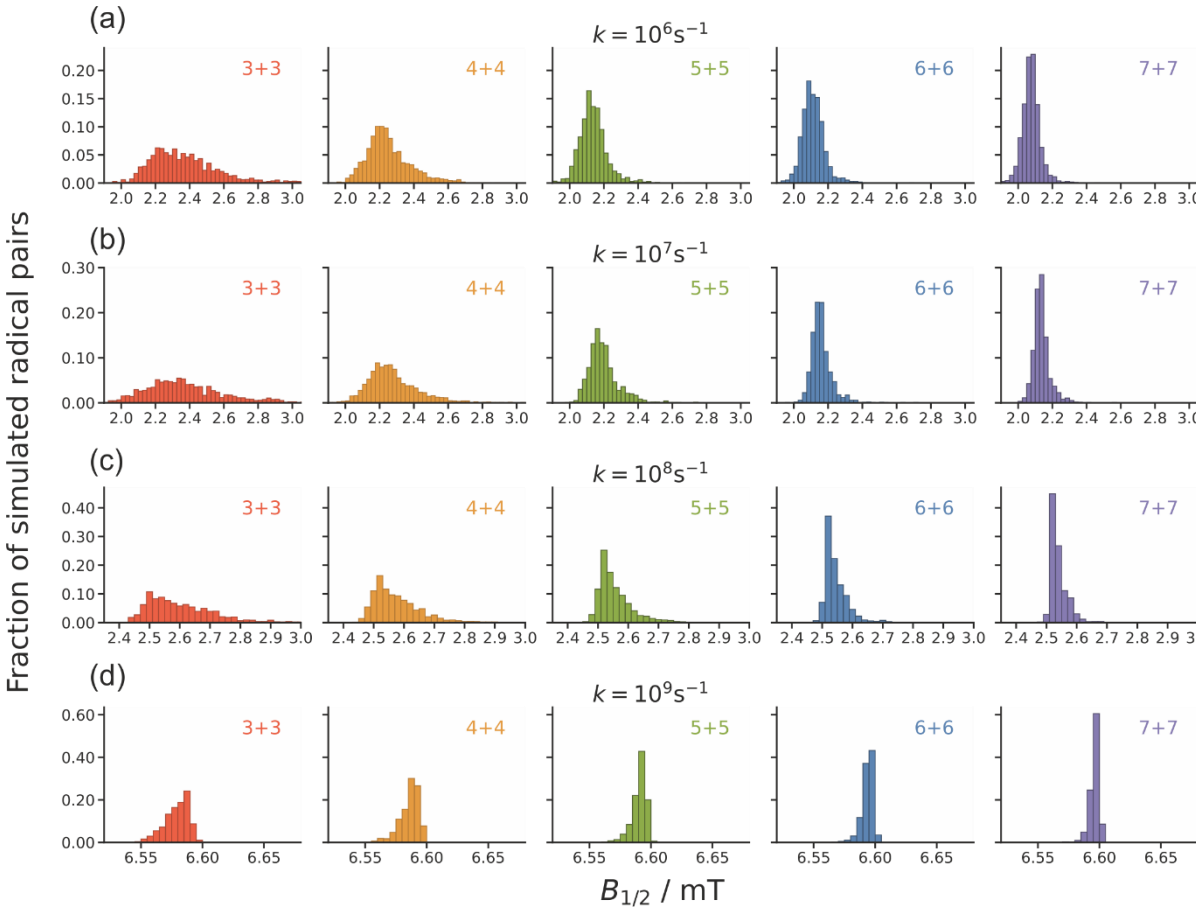

Fig. S7. $B_{1/2}$ distributions calculated using the QMMC method for model [$FAD^{\bullet-}$ $TrpH^{\bullet+}$] radical pairs containing 3, 4, 5, 6, or 7 hyperfine interactions per radical, as indicated. The recombination rate constant, k, is (a) 10^6 s^{-1}, (b) 10^7 s^{-1}, (c) 10^8 s^{-1}, and (d) 10^9 s^{-1}. Panel (a) is a duplicate of Fig. 3 in the main text.

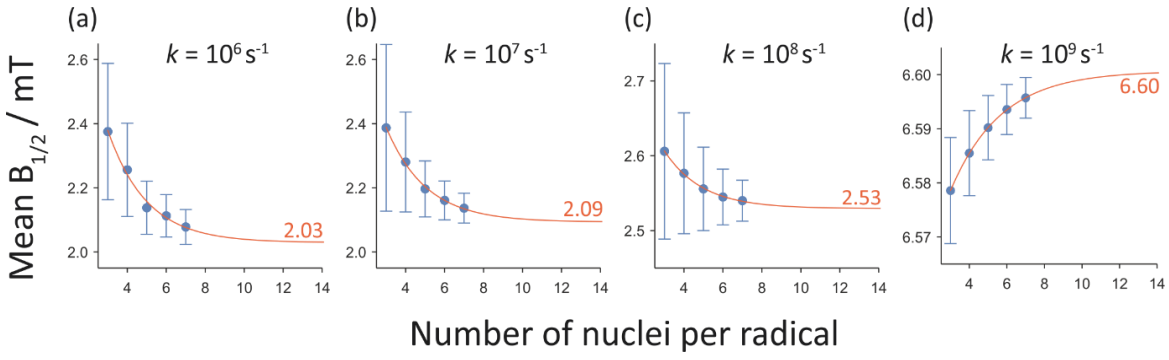

Fig. S8. Exponential extrapolation of the means of the $B_{1/2}$ distributions in Fig. S7.

S7. Simulated magnetic field effects: QD method

Field-dependence of $\Phi_T(B)$

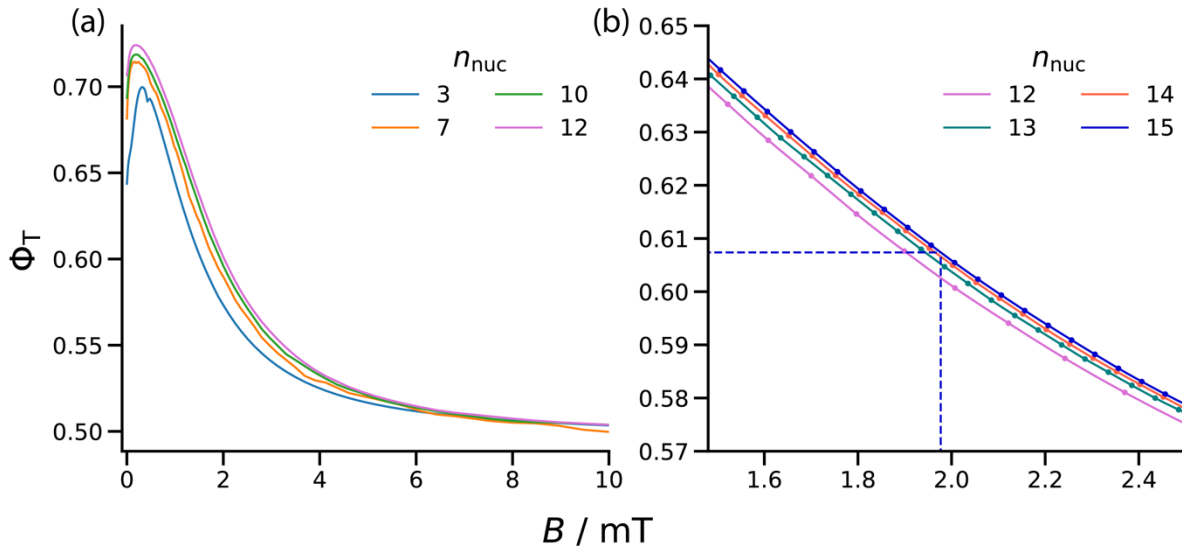

Fig. S9. Magnetic field effects (QD method) from which the $B_{1/2}$ values in Fig. 4a were obtained by interpolation for model [$FAD^{\bullet-}$ $TrpH^{\bullet+}$] radical pairs with $k = 10^6$ s^{-1} and (a) n_{nuc} = 3, 7, 10, 12 and (b) n_{nuc} = 12 – 15. Only the region between B = 1.48 mT and B = 2.52 mT is shown in (b) for clarity. Solid lines indicate the 3rd degree spline fits to calculated values of Φ_T (B), which are indicated as dots in (b) but omitted in (a) due to the large number (500) of points. The dashed line in (b) indicates the interpolation used to obtain $B_{1/2}$ for n_{nuc} = 15.

Extrapolation of $B_{1/2}$ to $n_{\mathrm{nuc}} \to \infty$

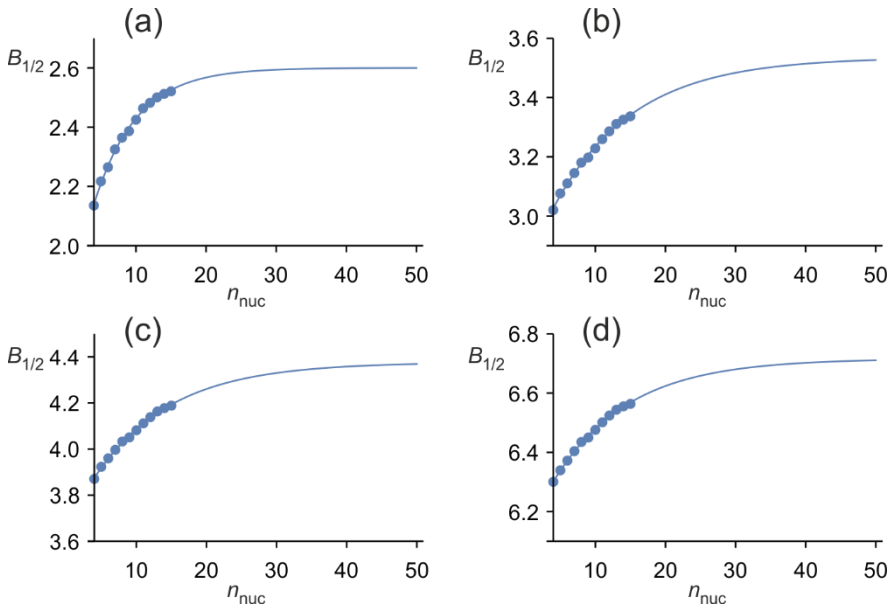

Fig. S10. QD values of $B_{1/2}$ in Fig. 4a extrapolated exponentially to $n_{\mathrm{nuc}} \to \infty$. (a) $k = 1 \times 10^8$, (b) $k = 3 \times 10^8$, (c) $k = 5 \times 10^8$, (d) $k = 1 \times 10^9$ s^{-1}.

S8. Simulated magnetic field effects: SC method

Interpolation to obtain $B_{1/2}$

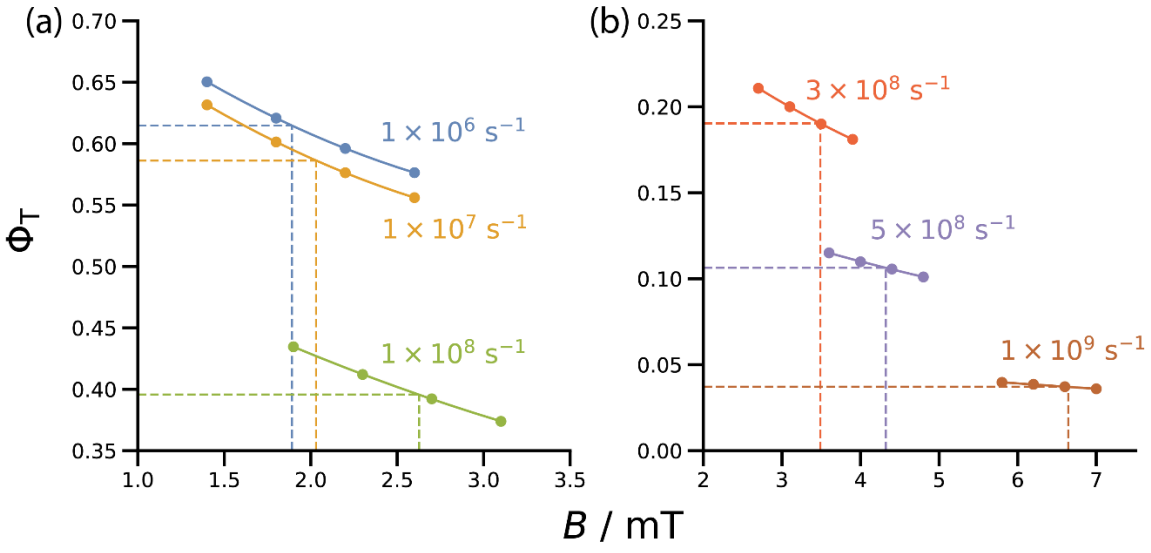

Fig. S11. Magnetic field effects (SC method) for model [FAD$^{\bullet-}$ TrpH$^{\bullet+}$] radical pairs, corresponding to the $n_{\mathrm{nuc}} = 27$ points for the six rate constants shown in Fig. 4a. (a) $k = 10^6$, 10^7, 10^8 s^{-1}. (b) $k = 3 \times 10^8$, 5×10^8, 10^9 s^{-1}. Solid lines indicate the 2$^{\mathrm{nd}}$ order polynomial fits to the calculated values of Φ_T (B) (dots). The interpolations used to obtain $B_{1/2}$ are indicated by dashed lines.

Comparison of $B_{1/2}$ from SC and QD methods

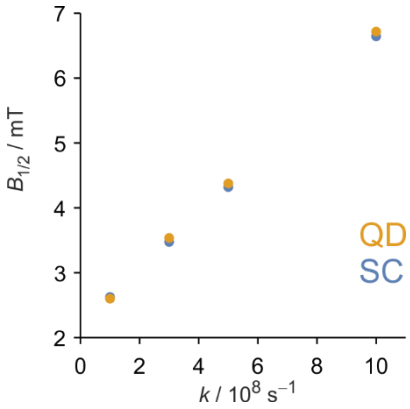

Fig. S12. Comparison of $B_{1/2}$ calculated with $n_{\mathrm{nuc}} = 27$ using the SC method with the QD values extrapolated exponentially from $n_{\mathrm{nuc}} = 4$-15 to $n_{\mathrm{nuc}} \to \infty$.

S9. Simulated magnetic field effects: *SU*(*Z*) method

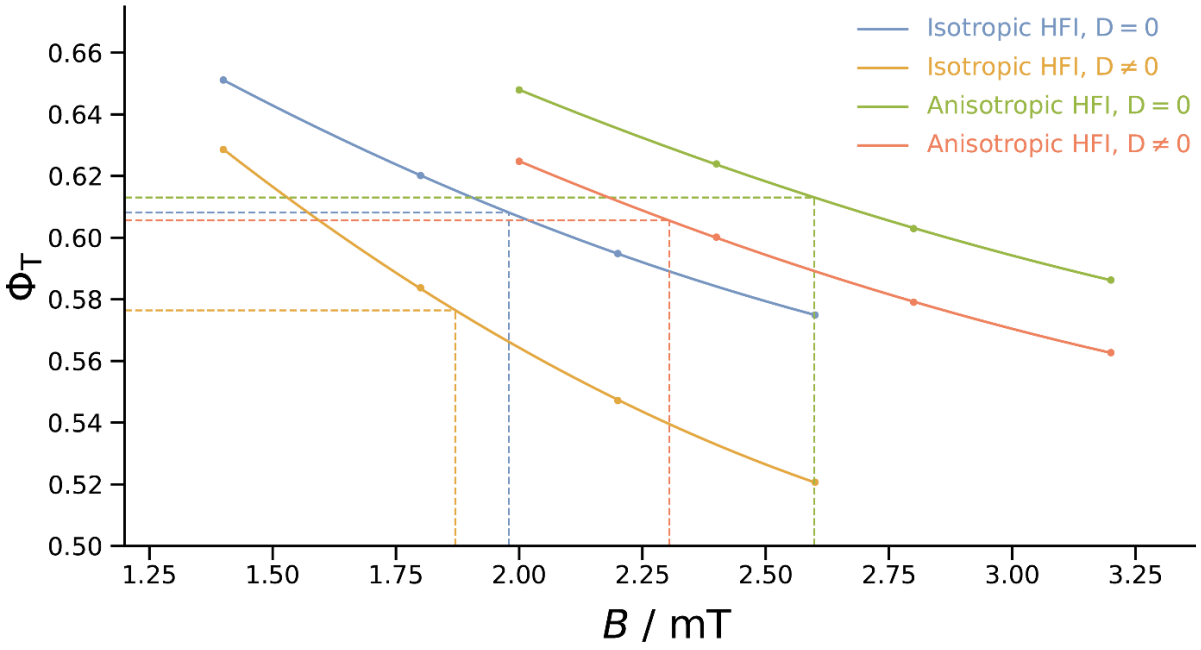

Fig. S13. Magnetic field effects (*SU*(*Z*) method) for k = 10^6 s^{-1} for model [FAD$^{\bullet-}$ TrpH$^{\bullet+}$] radical pairs, corresponding to the n_{nuc} = 16 points shown in Fig. 5. Solid lines indicate the 2$^{\mathrm{nd}}$ order polynomial fits to calculated values of Φ_T (B) (dots). The interpolations used to obtain $B_{1/2}$ are indicated by dashed lines.

S10. Estimate of τ_c for Cry4a

The rotational correlation time of an approximately spherical globular protein can be estimated using Stokes' law:[13]

$$\tau_c = \frac{4\pi\eta r_H^3}{3k_B T} \quad (1)$$

where η is the viscosity of the solvent and T is the temperature. r_H, the effective hydrodynamic radius, may be estimated from the specific volume of the protein, V, and the thickness of its hydration layer, r_W:[13]

$$r_H = \left(\frac{3VM}{4\pi N_A}\right)^{1/3} + r_W, \quad (2)$$

where M is the molar mass of the protein. Following Ref. [13] (eqns (1.44) and (1.45), page 21), we use $V = 7.3 \times 10^{-4}$ m^3 kg^{-3} and $r_W = 1.6 \times 10^{-10}$ m. For Cry4a (M = 64 kg mol^{-1}) in 80:20 water:glycerol at 5° C (Ref. [14]), $\eta = 3.2 \times 10^{-3}$ J s m^{-3} (Ref. [15]). Hence:

$$r_H = 2.81\,\text{nm} \quad \text{and} \quad \tau_c = 77.1\,\text{ns}. \quad (3)$$

References

1. A. Weller, F. Nolting and H. Staerk, *Chem. Phys. Lett.*, 1983, **96**, 24-27.
2. M. J. Frisch, G. W. Trucks, H. B. Schlegel, G. E. Scuseria, M. A. Robb, J. R. Cheeseman, J. A. Montgomery, T. V. Jr., K. N. Kudin, J. C. Burant, J. M. Millam, S. S. Iyengar, J. Tomasi, V. Barone, B. Mennucci, M. Cossi, G. Scalmani, N. Rega, G. A. Petersson, H. Nakatsuji, M. Hada, M. Ehara, K. Toyota, R. Fukuda, J. Hasegawa, M. Ishida, T. Nakajima, Y. Honda, O. Kitao, H. Nakai, M. Klene, X. Li, J. E. Knox, H. P. Hratchian, J. B. Cross, C. Adamo, J. Jaramillo, R. Gomperts, R. E. Stratmann, O. Yazyev, A. J. Austin, R. Cammi, C. Pomelli, J. W. Ochterski, P. Y. Ayala, K. Morokuma, G. A. Voth, P. Salvador, J. J. Dannenberg, V. G. Zakrzewski, S. Dapprich, A. D. Daniels, M. C. Strain, O. Farkas, D. K. Malick, A. D. Rabuck, K. Raghavachari, J. B. Foresman, J. V. Ortiz, Q. Cui, A. G. Baboul, S. Clifford, J. Cioslowski, B. B. Stefanov, G. Liu, A. Liashenko, P. Piskorz, I. Komaromi, R. L. Martin, D. J. Fox, T. Keith, M. A. Al-Laham, C. Y. Peng, A. Nanayakkara, M. Challacombe, P. M. W. Gill, B. Johnson, W. Chen, M. W. Wong, C. Gonzalez and J. A. Pople, Gaussian, Inc., Wallingford, CT, revision C.02 edn., 2004.
3. A. A. Lee, J. C. S. Lau, H. J. Hogben, T. Biskup, D. R. Kattnig and P. J. Hore, *J. R. Soc. Interface*, 2014, **11**, 20131063.
4. K. Schulten and P. G. Wolynes, *J. Chem. Phys.*, 1978, **68**, 3292-3297.
5. K. Maeda, T. Miura and T. Arai, *Mol. Phys.*, 2006, **104**, 1779-1788.

6. C. R. Timmel, U. Till, B. Brocklehurst, K. A. McLauchlan and P. J. Hore, *Molec. Phys.*, 1998, **95**, 71-89.
7. U. Till, C. R. Timmel, B. Brocklehurst and P. J. Hore, *Chem. Phys. Lett.*, 1998, **298**, 7-14.
8. C. Nielsen and I. A. Solov'yov, *J. Chem. Phys.*, 2019, **151**, 194105.
9. D. E. Manolopoulos and P. J. Hore, *J. Chem. Phys.*, 2013, **139**, 124106.
10. T. P. Fay, L. P. Lindoy, D. E. Manolopoulos and P. J. Hore, *Faraday Discuss.*, 2020, **221**, 77-91.
11. T. P. Fay, L. P. Lindoy and D. E. Manolopoulos, *J. Chem. Phys.*, 2021, **154**, 084121.
12. C. Lanczos, *J. Res. Nat. Bur. Stand.*, 1950, **45**, 255-282.
13. J. Cavanagh, W. J. Fairbrother, A. G. Palmer, M. Rance and N. J. Skelton, *Protein NMR Spectroscopy. Principles and Practice*, Elsevier Academic Press2007.
14. J. Xu, L. E. Jarocha, T. Zollitsch, M. Konowalczyk, K. B. Henbest, S. Richert, M. J. Golesworthy, J. Schmidt, V. Déjean, D. J. C. Sowood, M. Bassetto, J. Luo, J. R. Walton, J. Fleming, Y. Wei, T. L. Pitcher, G. Moise, M. Herrmann, H. Yin, H. Wu, R. Bartölke, S. J. Käsehagen, S. Horst, G. Dautaj, P. D. F. Murton, A. S. Gehrckens, Y. Chelliah, J. S. Takahashi, K.-W. Koch, S. Weber, I. A. Solov'yov, C. Xie, S. R. Mackenzie, C. R. Timmel, H. Mouritsen and P. J. Hore, *Nature*, 2021, **594**, 535-540.
15. http://www.met.reading.ac.uk/~sws04cdw/viscosity_calc.html.